Original Research

Control of oxygen tension recapitulates zone-specific functions in human liver microphysiology systems

Felipe T Lee-Montiel[1,*], Subin M George[1,2,*], Albert H Gough[1,2,*], Anup D Sharma[1,2], Juanfang Wu[1], Richard DeBiasio[1], Lawrence A Vernetti[1,2] and D Lansing Taylor[1,2,3]

[1]Drug Discovery Institute, University of Pittsburgh, Pittsburgh, PA 15260, USA; [2]Department of Computational and Systems Biology, University of Pittsburgh, Pittsburgh, PA 15260,USA; [3]Pittsburgh Cancer Institute, University of Pittsburgh, Pittsburgh, PA 15260, USA
*These authors contributed equally to this article.
Corresponding author: Albert H Gough. Email: gough@pitt.edu

Impact statement

Oxygen zonation is a critical aspect of liver functions. A human microphysiology system is needed to investigate the impact of zonation on a wide range of liver functions that can be experimentally manipulated. Because oxygen zonation has such diverse physiological effects in the liver, we developed and present a method for computationally modeling and measuring oxygen that can easily be implemented in all MPS models. We have applied this method in a liver MPS in which we are then able to control oxygenation in separate devices and demonstrate that zonation-dependent hepatocyte functions in the MPS recapitulate what is known about *in vivo* liver physiology. We believe that this advance allows a deep experimental investigation on the role of zonation in liver metabolism and disease. In addition, modeling and measuring oxygen tension will be required as investigators migrate from PDMS to plastic and glass devices.

Abstract

This article describes our next generation human Liver Acinus MicroPhysiology System (LAMPS). The key demonstration of this study was that Zone 1 and Zone 3 microenvironments can be established by controlling the oxygen tension in individual devices over the range of ca. 3 to 13%. The oxygen tension was computationally modeled using input on the microfluidic device dimensions, numbers of cells, oxygen consumption rates of hepatocytes, the diffusion coefficients of oxygen in different materials and the flow rate of media in the MicroPhysiology System (MPS). In addition, the oxygen tension was measured using a ratiometric imaging method with the oxygen sensitive dye, Tris(2,2′-bipyridyl) dichlororuthenium(II) hexahydrate (RTDP) and the oxygen insensitive dye, Alexa 488. The Zone 1 biased functions of oxidative phosphorylation, albumin and urea secretion and Zone 3 biased functions of glycolysis, α1AT secretion, Cyp2E1 expression and acetaminophen toxicity were demonstrated in the respective Zone 1 and Zone 3 MicroPhysiology System. Further improvements in the Liver Acinus MicroPhysiology System included improved performance of selected nonparenchymal cells, the inclusion of a porcine liver extracellular matrix to model the Space of Disse, as well as an improved media to support both hepatocytes and non-parenchymal cells. In its current form, the Liver Acinus MicroPhysiology System is most amenable to low to medium throughput, acute through chronic studies, including liver disease models, prioritizing compounds for preclinical studies, optimizing chemistry in structure activity relationship (SAR) projects, as well as in rising dose studies for initial dose ranging.

Keywords: Liver, zonation, oxygen, microphysiology systems

***Experimental Biology and Medicine* 2017; 242: 1617–1632. DOI: 10.1177/1535370217703978**

Introduction

The human body functions over a broad range of oxygen (O_2) concentrations that are required for specific organ functions. The liver is composed of approximately 100,000 small hexagonal structural units known as lobules. At the periphery of these lobules, oxygenated blood from the portal venules and the hepatic arterioles enters the sinusoids where oxygen is consumed, principally by the hepatocytes, forming an O_2 gradient (zonation).[1] Multiple factors including O_2 concentration, hormone gradients, nutrients, matrix composition, and the distribution of non-parenchymal cells are thought to contribute to hepatocyte zonation.[2] Metabolically, the functional unit of the liver is the hepatic acinus, which can be divided into three Zones: Zone 1 periportal (PP), Zone 2 transitional, and Zone 3 perivenous (PV) (Figure 1).[3] The periportal Zone 1 is supplied with highly oxygenated blood ($pO_2 \approx 60$–70 mmHg ≈ 10–12%), whereas the perivenous Zone 3 is proximal to the central vein and receives oxygen depleted blood ($pO_2 \approx 25$–35 mmHg ≈ 3–5%).[4] Despite the important role of

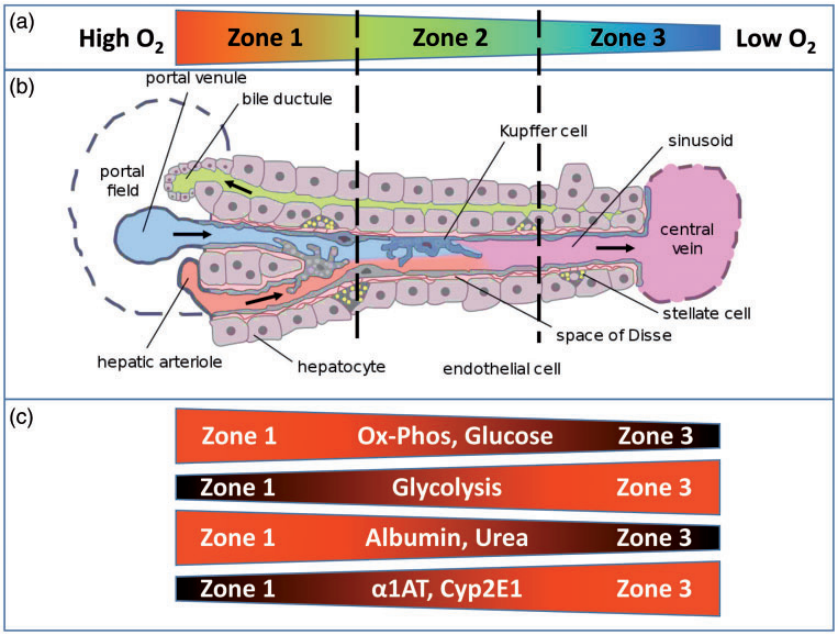

Figure 1 Functional activity in the liver acinus varies with oxygen zonation. The liver acinus exhibits a decreasing oxygen gradient from the portal venule to the central vein. Some cellular functions like oxidative phosphorylation and secretions (albumin and urea) follow the gradient, while other functions like Cyp2E1 activity and α1AT secretion run opposite to the oxygen gradient. Illustration adapted from Frevert *et al*.[3]

zonation in modulating liver functions, no human microphysiology system (MPS) replicates the microenvironments found in the different sinusoidal zones.

Oxygen zonation in the liver impacts multiple cellular functions including: carbohydrate, amino acid and lipid metabolism; energy metabolism (oxidative phosphorylation and glycolysis); drug metabolism; protein synthesis; autophagy; antioxidative mechanisms; and others.[5] Because oxygen zonation has such diverse physiological effects, liver MPS models must address oxygenation and incorporate monitoring and control of the oxygen tension. Furthermore, experiments in which oxygenation is controlled or manipulated should take into account the time required for zonal physiological changes to occur.

Oxygen zonation also plays a role in disease progression, although our understanding of the relationship between liver diseases and zonation is limited.[6] Periportal fibrosis is found in approximately 30% of cystic fibrosis patients providing one clear example where the location of the early stage liver disease is restricted to a single liver Zone.[7] The genetic defect accounting for the loss or dysfunction of the cystic fibrosis transmembrane conductance regulator (CFTR) chloride channel is found in portal triad cholangiocytes.[7] The disease obstructs bile flow, induces local inflammation followed by the activation of hepatic stellate cells, which ends in progressive fibrosis.[7] Another example of the role of zonation in a disease involves the Wnt/β-catenin signaling pathway as the master regulator of zonation.[8,9] This pathway is of interest in a type of well-differentiated hepatocellular carcinoma in which high levels of mutant β-catenin activation are found in the perivenous region (Zone 3).[9–11] The Wnt/β-catenin pathway may also be responsible for the switching of Zone 2 to Zone 1 early in the infection of hepatocytes by low levels of HCV virus in mouse models.[12] Finally, evidence suggests the zonation dependence of protein, glucose and lipid metabolism may have important implications in the pathogenesis of nonalcoholic steatohepatitis (NASH).[13]

It is therefore important for MPS models of liver and other organs to mimic as close as possible the *in vivo* physiological environment in terms of oxygenation, as well as nutrient supply, chemical gradients, mechanical forces, cellular composition and architecture, in order to achieve more relevant differentiated cellular phenotypes and functions.[14,15] Optimally, constructed organs-on-chips (MPS) comprising the proper human cell types, assembled in a relevant tissue architecture and growing under physiological conditions should behave like the functional units of organs in the human body, making them powerful *in vitro* models for studying diseases and drug testing.[16,17] When compared to animal models, these MPS models are expected to be more relevant to the human, less expensive, more reproducible, and can be tailored to specific organ functions. In the case of the liver, most of the liver MPS address specific properties of the liver without regard to zonation. For example, there are MPS models focused on collection of bile,[18] improved microscale architecture,[19] embedded microvascular systems,[20] or large scale hepatocyte culture.[21] However, zonal differences in hepatocyte physiology must be considered in developing liver MPS. For example, MPS liver models are often evaluated based on levels of albumin and urea synthesis, which are higher in the periportal Zone, as well as levels of Cyp450 expression, which are higher in the perivenous Zone. There is no evidence that hepatocytes can simultaneously exhibit both phenotypes.[4] There are microfluidic liver models that incorporate oxygen gradients using perfusion in flat plate bioreactors;[22–25] however, the 2D hepatocyte cultures

in these reactors lead to loss of key functions after only a few days.[4] An optimal 3D, multicellular liver MPS with the ability to control the microenvironment to create distinct zonation is clearly advantageous for studying liver physiology, liver diseases, testing compounds for toxicity and for coupling to other organ MPS.[26]

In MPS models, oxygen can enter the system by two means – diffusion through the materials, and through media exchange. Polydimethylsiloxane (PDMS) is routinely used for prototyping models because it is easy to fabricate and is oxygen permeable.[27] However, PDMS absorbs hydrophobic compounds, limiting the ability to test them in most MPS.[28] Significantly, devices can be fabricated in plastics that will bind far less of a hydrophobic compound; however, most plastics are oxygen impermeable making it more challenging to provide sufficient oxygen. Poly(methyl pentene) is a promising new plastic for fabricating devices with some oxygen permeability,[29] although its compound adsorption properties have not been well characterized. Dissolved oxygen also enters MPS models during media exchange or flow. Oxygen is depleted in MPS models through the consumption of oxygen by the cells, and oxygen in the effluent. The consumption can be affected by the cell density, as well as by the cell type (e.g. hepatocytes consume much more oxygen than endothelial cells). The balance between the net oxygen entering the system and the oxygen consumption by the cells determines the final steady state oxygen tension. Computational modeling and measuring of oxygen in the MPS are required to determine whether the cells in an MPS are in a normoxic, hypoxic or hyperoxic environment, preferably with temporal and spatial resolution.

In this study, we present our next generation, 3D, Liver Acinus MPS (LAMPS), an extension of our first liver MPS,[17] with improved acinus structure and cellular composition, in a commercial device consisting of glass, PDMS and plastic.[17] The first improvement was the addition of a thin extracellular matrix on the hepatocytes to mimic the Space of Disse. The Space of Disse is a protein-rich interface that creates a permeable layer in the sinusoidal lumen, which is covered by fenestrated endothelial cells and rests on the basolateral surface of hepatocytes. It has a crucial function to allow direct contact of blood plasma and unimpeded transfer of signaling molecules, xenobiotics and nutrients to the hepatocytes.[30,31] Furthermore, the space of Disse contains hepatic stellate cells and is the location for life threatening liver pathologies such as fibrosis and cirrhosis.[32,33] Second, the LAMPS in this study used primary human endothelial cells along with primary human hepatocytes, a stellate cell line and Kupffer-like immune cells. The development of the LAMPS model has been evolutionary, and while the goal is to use all primary human liver-derived cells, or patient iPS-derived cells, the cells used here provided a robust model on which to evaluate control of oxygenation and it's effect on hepatocyte functions.

To address oxygenation in the LAMPS, we developed a computational model of oxygen flows in the device, including media transport, material permeability and cellular consumption, which showed that oxygen could be controlled within physiological limits, ~0–15%, by slightly varying the media flow rate in the device. To verify the results of the modeling, we used oxygen sensitive and insensitive fluorophores in a ratiometric approach to measure dissolved oxygen temporally and spatially within the MPS under defined flow conditions. Consistent with the model, we confirmed that flow rates of 15 μL/h and 5 μL/h resulted in oxygen tensions comparable to Zones 1 and 3, respectively. We demonstrated zonation-dependent liver functions including oxidative phosphorylation, glucose metabolism, albumin, urea and α1-antitrypsin secretion, Cyp2E1 expression, steatosis and acute acetaminophen toxicity. The results presented here demonstrate that the LAMPS can be used to model and measure defined oxygen Zones in the liver, to investigate zone-specific liver metabolism and disease. In addition, the methods can be applied to a wide range of organ MPS.

Materials and methods

Cells sources

A single lot of cryopreserved primary human hepatocytes (lot# Hu8130) with >90% viability and re-plating efficiency post thaw, was selected from Life Technologies (Grand Island, NY). Human dermal microvascular endothelial cells (HMVEC-D) were purchased from Lonza (Walkersville, MD) and transformed liver endothelial cells, TMNK-1, were kindly provided by Prof. Alejandro Soto-Gutierrez (University of Pittsburgh). Human umbilical vein endothelial cells, EA.Hy926 and human histolytic lymphoma (human monocyte) cells, U937, were obtained from ATCC (Manassas, VA). Monocytic leukemia cells from peripheral blood (human monocyte), THP-1, were generously provided by the Center for Vaccine Research, Pittsburgh, PA (also available from ATCC). Human stellate cells, LX-2, were originally provided by Martin Yarmush, Massachusetts General Hospital are also available from EMD Millipore (Billerica, MA). The LX-2 cell is an immortalized human hepatic stellate cell that constitutively expresses key receptors regulating hepatic fibrosis, and proliferates in response to PDGF, a prominent mitogen contributing to liver fibrosis.[34,35]

Primary human hepatocytes were cultured in hepatocyte maintenance media (HMM) consisting of 96% William E medium (Life Tech, A12176-01), 4% cocktail B (Life Tech, A13448) and 10 mM Dexamethasone 1 μl/100 ml medium (Life Tech, A13449). LAMPS perfusion media consisted of HMM + 1% fetal bovine serum (FBS) + 10 ng/mL vascular endothelial growth factor (VEGF) (PHC9394, Fisher Scientific) + 50 μg/mL porcine liver extracellular matrix (LECM). All perfusion media was equilibrated to atmospheric oxygen, and therefore contained 18% dissolved oxygen.[29,36,37]

Monocyte differentiation

U937 and THP-1 cells were differentiated into mature macrophages by treatment with 200 ng/mL phorbol myristate acetate for 48 h. Differentiated U937 macrophages and THP-1 monocytes release human tumor necrosis factor alpha (TNF-α) and IL-6 in response to LPS treatment,

a condition reported to induce the immune mediated liver toxic response in *in vitro* and *in vivo* models.[17,38,39]

LAMPS assembly and maintenance

A single chamber commercial microfluidic device (HAR-V single channel device, SCC-001, Nortis, Inc. Seattle, WA) was selected for optical quality for imaging and robust mechanical design (Supplemental Figure S1). The devices were stored in phosphate-buffered saline (PBS) until use. The interior of the devices was dried under vacuum prior to protein coating with 100 μg/mL bovine fibronectin and 150 μg/mL rat tail collagen, type 1, alpha 2 in PBS as previously described.[17] For all steps involving injection of fluid (media, cell suspension, etc.) into the devices, 100–150 μl per device was used to ensure complete filling of fluidic pathways, chamber and bubble traps. Cryopreserved hepatocytes were thawed following the manufacturer's recommendations. Hepatocytes were pelleted at $100 \times g$ for 3 min, resuspended at 2.75×10^6 hepatocytes/mL in Williams E medium supplemented with 5% fetal bovine serum (Cellgro, Manassas CA), 100 μg/mL Penicillin Streptomycin (HyClone, Logan, UT) and 2 mM L-glutamine, then injected into the interstitial compartment of the device for overnight incubation at 37°C to allow adherence and spreading. Plating media was removed from the device and a solution of 400 μg/ml of porcine LECM[40] (provided by Dr. Stephen Badylak's lab, University of Pittsburgh) in hepatocyte maintenance media (HMM) (Life Technology, Grand Island, NY) was added and incubated for 3 h at 37°C to create a thin matrix layer on top of the hepatocytes. A mixture of 3.0×10^6 HMVEC-D cells/mL and 0.8×10^6 THP-1 monocytic cells/mL in EGM-2 (Lonza) was then sequentially injected on top of the LECM, and incubated for 2 h at 37°C before the final injection of 0.4×10^6 LX-2 cells suspended in 1 mL of a 2.5 mg/mL solution of pH 7.2 rat tail collagen/10 mM HEPES/HBSS. The devices were inverted for 1 h at 37°C during collagen polymerization to ensure an initial spatial separation of hepatocytes and stellate cells. The devices were re-inverted to their normal orientation and incubated overnight to allow stabilization of the model before initiating 5 and 15 μL/hour perfusion with HMM + 10 ng/ml VEGF supplemented with 100 nM dexamethasone and 50 μg/ml of porcine LECM at 37°C in 5% CO_2 humidified atmosphere.

Perfusion rates required to achieve target oxygen concentrations were determined with a finite element computational model in COMSOL Multiphysics 5.2 (Comsol, Inc., Burlington, MA). Syringe pumps (KD Scientific, Holliston, MA) and 10 ml plastic syringes were used to perfuse the microfluidic devices at desired flow rates in a humidified tissue culture incubator (37°C in 5% CO_2). Two days were required to assemble and to stabilize the liver MPS. Perfusion was then initiated (called day 0) to start the experiments.

Establishing Zone 1 and Zone 3 microenvironments in individual live MPS

To test zone specific physiology, liver MPS were maintained either at 15 μl/h to create Zone 1 or at 5 μl/h to create Zone 3. The MPS were incubated for five days to ensure the establishment of Zone 1 and Zone 3 oxygen tensions prior to physiological/molecular characterization (see below).

Sample collection and biochemical measurements

Effluent media was collected in tubes every two days for 14 days and frozen at −20°C for subsequent analysis for albumin, urea, lactate dehydrogenase (LDH), TNF-α and α-1-antitrypsin (α1AT) synthesis. Albumin was measured using an enzyme linked immunosorbent assay (Bethyl Laboratories, Montgomery TX). LDH and urea nitrogen were measured using colorimetric assays (CytoTox 96, Promega, Madison, WI, and Urea Nitrogen Test, Stanbio Laboratory, respectively). ELISA kits for human TNF-α (ThermoFisher, Pittsburgh, PA) and α1AT chemiluminescence (RayBiotech, Norcross, GA) were used per the manufacturer's guidelines. All biochemical assays of the efflux media were performed in 96- or 384-well microplates according to manufacturer's instructions, with the exception of the blood urea nitrogen (BUN) assay, which was modified from the manufacturer's protocol by reconfiguring for a 384-well microplates and increasing the incubation time for reactants from 60 to 90 min at 60°C before reading. All biochemical assays were analyzed in 10 μL of media per readout and measured on a SpectraMax M5 microplate reader (Molecular Devices, Sunnyvale CA). All sample results were calculated by interpolation of sample values from standard curves performed in parallel.

Confocal imaging

The Nortis microfluidic devices have a coverslip thick glass bottom for imaging cells both live and fixed. Imaging experiments were performed using the IN Cell Analyzer 6000 (GE Healthcare, Piscataway, NJ) system. The confocal sections used to construct the cross-sectional image of the cells in the MPS were acquired on a CSU-10-ML spinning disk confocal (Solamere Technology Group, Salt Lake City, UT) using a 25 × (1.0 NA) water immersion objective to collect 50 μm stacks at 0.5 μm spacing from 30 adjacent fields. The stacks were stitched to create a cross-sectional projection that established the distribution of the cells in the assembled model. Hepatocytes were labeled with a cytochrome-c biosensor,[17,41] a rhodamine-labeled fibronectin (Cytoskeleton, Inc., Denver, CO) was diluted 1:10 (final concentration of 40 μg/mL) in the LECM (400 μg/mL) and the HMVEC-D cells were labeled with a 1:100 dilution in PBS of primary antibody to CD31 (Clone WM59,BD Biosciences) followed by a 1:100 dilution in PBS of Cy5 labeled secondary (Cy5-donkey anti-mouse IGG, Jackson ImmunoResearch Labs). Following overnight labeling, devices were washed twice in 1 × PBS for 10 min, and stored in PBS at 4°C.

Modeling oxygen tension

Oxygen tension in the LAMPS was computationally modeled using COMSOL Multiphysics v5.2. A CAD model of the device was provided by Nortis, Inc. The Comsol modules for *Free and Porous Media Flow* and *Transport of Dilute*

Species were used to model flow and diffusion, respectively, using the parameters listed in Supplementary Table S1. The bottom glass base was treated as oxygen impermeable, while the side and top channel walls were modelled as PDMS with an inward oxygen flux of 3.25 e-9 moles/m^2/s[42] occurring at the PDMS-media boundary. Hepatocytes on the collagen-fibronectin coating were modelled as a thin 25-μm layer on the glass base of the device. Oxygen consumption in this layer was modelled using Michaelis–Menten kinetics in the COMSOL model. The Michaelis–Menten equation[42] is

$$R_{O_2} = \frac{V_{\max} C_{O_2}}{K_m + C_{O_2}} \rho_{cell} \quad (1)$$

where V_{max} and K_m are the oxygen kinetic parameters listed in supplementary Table S1 and ρ_{cell} is the overall cell density. The remaining space was modelled as filled with hydrogel with an initial O_2 concentration of 18%.[29,36,37]

A range of oxygen consumption rates (OCR) for hepatocytes (0.3–0.9 nmol/s/10^6 cells) have been reported in the literature.[43–45] To examine the effect of varying OCR, values ranging from 0.375 to 0.45 nmol/s/10^6 cells were used in the COMSOL simulation. To explore the variability in cell seeding density in the Nortis device, simulations were run for cell numbers of 50,000, 60,000, and 70,000 cells/device. The flow rates used in the simulation were 0, 5 and 15 μL/h. Cell seeding densities and the 5 μl/h flow rate were based on previous work that used a prototype version of the Nortis microfluidic device used here.[17] COMSOL simulations indicated that a 5 μl/h flow rate created zone 3 oxygen tensions, while a 15-μl/h flow rate created zone 1 oxygen tension. Media flowing into the MPS was considered to have been equilibrated with atmospheric oxygen and therefore containing 18% dissolved oxygen.[29,36,37] The simulations in all cases were run using a coarse mesh to model 18 h of flow at 1-h intervals. The COMSOL simulations were also used to evaluate the maximum shear stresses that are generated inside the LAMPS, 20 μm above the glass surface, for 5, 15 and 50 μL/h.

Measuring oxygen tension

Oxygen tension was measured by ratio imaging of a solution of the oxygen sensitive dye Tris(2,2′-bipyridyl) dichlororuthenium(II)hexahydrate (RTDP) (Catalog #544981-1 G, Sigma Aldrich) with the oxygen insensitive dye Alexa Fluor® 488 Carboxylic Acid, tris(triethylammonium) salt (Alexa 488) (Catalog #A33077, Life Technologies) (Supplemental Figure S2) in order to normalize the measurements for any variations in pathlength and other optical perturbations.[46] Glucose oxidase from Aspergillus niger Type VII, lyophilized powder was sourced from Sigma Aldrich (Catalog # G2133-10 KU). Stock solutions of 150 mM RTDP and 1 mg/mL Alexa 488 were prepared in PBS and stored at −20°C. For use in ratiometric oxygen measurements, the dyes were further diluted in HMM to final concentrations of 150 μM RTDP and 0.667 μg/ml Alexa 488.

A simplified LAMPS model consisting of primary human hepatocytes with collagen ECM matrix overlay was used to develop and test the oxygen measurements. Devices were pretreated with ECM as described earlier followed by plating with hepatocytes. After allowing hepatocytes to attach overnight, the device was filled with collagen which polymerized to form a collagen gel ECM that filled the remaining space in the chamber and microfluidic channels. Flow with HMM containing 18% dissolved oxygen was initiated at 5 μL/h or 15 μL/h the next day and devices were maintained under flow for two days to allow the cells in the model time to assemble before making oxygen measurements.

To measure oxygen, devices were transferred to the IN Cell Analyzer 6000 where the environmental chamber maintained 37°C for the course of the measurement. Devices were initially loaded with dye containing media at 200 μL/h for half an hour, then flow was ramped down to the target flow rate (5 or 15 μL/h) over a period of 20 min. Images were taken after 4 h at the target flow rate. When measurement imaging was complete, calibration images were taken on the same device. For calibration at 0% and 18% oxygen, flow with the respective calibration solution was initiated at 200 μL/h for half an hour to replace the media in the device before ramping down to the target flow rate (5 or 15 μL/h) over 20 min, followed by imaging. The 0% oxygen calibration solution included 0.2 mg/ml glucose oxidase, an oxygen scavenger, in HMM containing dye. The 18% oxygen calibration solution included 10 μM Antimycin A, an inhibitor of oxidative phosphorylation, in HMM containing dye. Both RTDP and Alexa 488 were imaged with a 488 nm laser excitation at 60% laser power, 20 × magnification, a 1.49 airy unit confocal slit width and a 1 s exposure. RTDP was imaged with a 605(40) nm emission filter and Alexa 488 was imaged with a 520(25) nm emission filter. Images were collected from 15 fields in the main chamber of each device, 80 μm above the coverslip glass bottom.

For each field, three RTDP/Alexa 488 intensity ratios were obtained – one after 4 h of flow at the target flow rate with live cells, one for 0% oxygen, and for 18% dissolved oxygen. The three ratiometric intensity values were used in the Stern–Volmer equation to calculate the oxygen concentration. The Stern–Volmer equation[47] is

$$\frac{I_0}{I} = 1 + K_q[O_2] \quad (2)$$

where I and I_0 are the fluorescence intensities at the given oxygen condition, $[O_2]$, and at 0% oxygen respectively. K_q is the Stern–Volmer constant calculated as

$$K_q = \frac{\frac{I_0}{I_{18}} - 1}{[O_2]_{air}} \quad (3)$$

where I_{18} is the fluorescence intensity at 18% oxygen (oxygen saturated media) and $[O_2]_{air}$ is 18%. Since a ratiometric approach was used, I was substituted as the ratio of RTDP Intensity to Alexa 488 Intensity, with I_0 and I_{18} being those measured at 0% and 18% Oxygen conditions. No

significant dye uptake into the cells occurred due to short duration of the presence of the dyes.

Steatosis measurements

Cells were fixed by injecting the devices with 4% paraformaldehyde in PBS for 30 min at room temperature then washed twice for 5 min with PBS + 1% bovine serum albumin (BSA). Following fixation, HCS LipidTOX™ Deep Red Neutral Lipid Stain (H34477, ThermoFisher Scientific) was injected to label lipid droplets for 2 h and then washed for 5 min with PBS. The devices were then imaged on the IN Cell Analyzer 6000 as a 3 × 5 array of adjacent fields covering an area 2 × 3.5 mm at 20 × magnification. Lipid droplets were identified by interactive selection of a threshold followed by watershed segmentation in FIJI.[48] The analyze particles function was used to measure the average area and count the lipid droplets with a size greater than 120 μm^2 in Zone 1 and Zone 3 liver MPS.

CYP2E1 measurements

LAMPS models were fixed in 4% paraformaldehyde in PBS for 30 min at room temperature, washed for 5 min with PBS while shaking, and then incubated in 0.15 M glycine in PBS for 30 min. Devices were then washed with PBS for 10 min, after which 0.5% Triton X-100 in PBS was added for 15 min to permeabilize the cellular membranes. Devices were then rinsed twice with PBS for 10 min and blocked for 1 h at 4°C with 1% fatty acid free BSA and 1% donkey serum in PBS. Devices were incubated overnight at 4°C with a primary antibody to Cyp2E1 (SAB1405688, Sigma) diluted (1:200) in PBS with 5% donkey serum. After labeling with the primary antibody, the devices were incubated overnight at 4°C with a Cy5-donkey anti-mouse antibody (Jackson ImmunoResearch Labs) using a 1:100 dilution in PBS with 5% donkey serum. Lastly, devices were washed twice in PBS for 10 min, and stored in PBS at 4°C. Immunostained devices were imaged at 20× on the IN Cell Analyzer 6000 as a 3 × 9 array of adjacent fields covering an area 2 × 6 mm. Images were segmented by interactive selection of a background threshold and analyzed field-by-field for average Cy5 intensity using FIJI. The resulting values were averaged.

Acetaminophen toxicity

Stock solutions of 5 M acetaminophen (Sigma, St. Louis, MO) were prepared from powder by dissolving in DMSO. These were diluted 1:500 in perfusion media to give the final concentration of 10 mM that was used for acute drug treatment. For drug free controls, DMSO was added 1:500 to perfusion media. After collecting the fifth day pretreatment efflux (time = 0 h), devices were subjected to either 10-mM drug treatment or controls (3 each per condition). Flow was initiated at 50 μL/h for all devices to rapidly exchange the chamber media. After 1 h, efflux was collected (time = 1 h) and then flow changed to 10 μL/h for all devices. Because this was an acute 5.5-h study, the hepatocytes were expected to maintain their functional state for the duration of the study, so a uniform media flow rate was used for all devices. Efflux was collected at three additional 1.5 h intervals (t = 2.5, 4.0, 5.5) for a total of 5.5 h of flow at 10 μL/h. The collected efflux was analyzed for LDH and the drug treated devices at each flow rate (5 or 15 μL/h) were normalized to their respective drug free controls.

Results

LAMPS: Next generation liver MPS

The previously published SQL-SAL 1.0 is a 3D microfluidic four human cell type liver MPS that partially recapitulated the organization of cells in the liver acinus, and successfully demonstrated multiple liver functions and responses to drug treatments, consistent with clinical studies.[17] However, the development of any organ MPS is an evolutionary process starting with some minimal level of sophistication and functionality with the strategy to increase the physiological significance.[17] The LAMPS improves on the architecture and function of the SQL-SAL 1.0 to enhance consistency with the human liver acinus. Table 1 compares the design of the SQL-SAL 1.0 with the LAMPS used in this study. Modifications were made to SQL-SAL 1.0 to measure and control oxygen tension and to establish Zone 1 and Zone 3 oxygen tension conditions, to improve the spreading of a primary human endothelial cell layer, and to increase the secretion of cytokines and growth factors by non-parenchymal cells.

Because of the importance of oxygen zonation in liver toxicology and disease, we will first address the modeling, measurement and control of oxygenation in the liver MPS, how those methods enable the recapitulation of specific oxygen Zones in individual LAMPS, and then show how the control of oxygenation in the MPS alters the physiology of the cells in a manner consistent with what is known about zonation dependent physiology in the human liver. The goal is to have liver MPS where Zone specific functions can be investigated (Figure 1).

Like SQL-SAL 1.0, LAMPS was constructed in a microfluidic chamber of about 50 μL volume illustrated in Figure 2(a), in a commercial Nortis device (Supplemental Figure S1). The four cell types were sequentially seeded in the chamber as described. To verify the layering of the cells in the chamber (Figure 2(b)), the liver MPS was constructed with hepatocytes expressing a GFP analog of cytochrome-c, LECM labeled with Cy3-fibronectin, and once the completed model had stabilized for several days, it was fixed and the endothelial cells were labeled with a CD-31 antibody, followed by a Cy5-secondary. Confocal imaging was used to collect a 3D set of images to evaluate the localization of the cells in the liver MPS. Figure 2(c) shows an X-Z section from the model that illustrates the layered organization of the hepatocytes (green), LECM layer (red) on the hepatocytes, with the endothelial cell layer (blue) on top. Overall thickness of the layers is about 12–15 μm (white scale bar is 10 μm).

Modeling O_2 tension in the LAMPS

Oxygen tension in the LAMPS is determined by the oxygen influx through the PDMS in the Nortis device, the

oxygen transported in the media, and the consumption of oxygen by the cells. Although all the cells consume oxygen, the hepatocytes are a major portion (40%) of the cells, and they consume 10 times more oxygen than the other cell types,[53,54] so estimates of oxygen consumption were calculated based on the hepatocytes. Of these parameters, the media flow rate is the easiest to control experimentally, and therefore we used COMSOL to model the oxygen tension as a function of media flow rate. The parameters used for the model are listed in Supplemental Table S1. Oxygen tension was calculated over an 18-h simulation period and a flow rate of 15 μL/h resulted in steady state oxygen level ranging between 12–15% (Figure 3(a)) while a 5 μL/h flow rate resulted in an oxygen level of 3–6% (Figure 3(b)) in the main chamber using reasonable published values in the computational model. Note that in both cases there is a shallow gradient in the chamber. The simulations in Figure 3(c) were run using 70,000 cells and an OCR of 0.45 nmol/s/10^6 cells.

It was important to evaluate the sensitivity of the COMSOL model to the cell number and OCR. Although counting the cells in the MPS chamber is consistent with

Table 1 Improvements in the LAMPS human liver on a chip

	SQL-SAL 1.0	LAMPS	Significance
Cell layering	Sequential layering of cells	LECM layer between hepatocytes and endothelial cells	Optimizes endothelial cell layer. (partial model of the space of Disse) Figure 1.
Flow rate	5 μl per hour	15 and 5 μl per hour for modelling Zone 1 and 3, respectively	Allows physiological range of oxygen tensions to be generated Figure 2
Oxygen monitoring	None	RTDP/Alexa 488 for real-time spatial and temporal oxygen monitoring	Quantifies on-chip oxygen tension to define Zone 1 and Zone 3 environments Figure 2, S2–S6, S8
Zone-based physiology	Zone 3 only	Zone 1 and Zone 3	Recapitulates physiology in Zones 1 and 3, Figures 3 to 5
NPC's			
Endothelial cells	EA.Hy926 (cell line)	HMVEC-D (Primary microvascular)	Higher secretion of cytokines, growth factors[49,50] and reduced proliferation[51]
Kupffer cells	U-937 (cell line)	THP-1 (cell line)	More stable differentiation[52] and higher levels of LPS stimulated TNF-α release S10
Stellate cells	LX-2 (cell line)	LX-2 (cell line)	Cells have performed well in the model, including demonstrating a fibrotic response[17,34]
Media	HMM	HMM with 1% FBS + 50 μg/ml soluble LECM	Newer formulation better supports NPC functions[44]

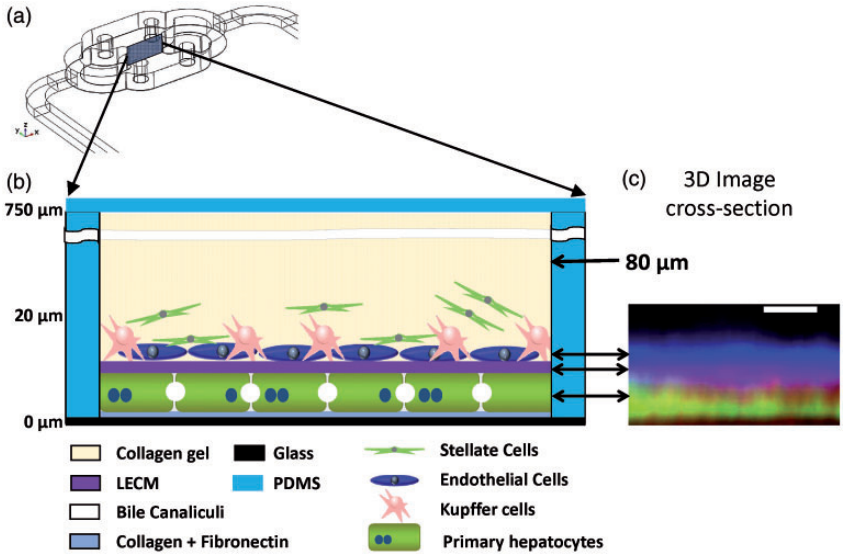

Figure 2 Structure of LAMPS (a) CAD drawing of the chamber in which the LAMPS model is constructed in the Nortis microfluidic device. (b) Illustration of the layering in the chamber, including (starting from the glass bottom): a layer of collagen and fibronectin; the hepatocyte layer; a layer of LECM; the endothelial and Kupffer cell layer; and stellate cells embedded in an overlaid collagen matrix. Arrow shows plane of oxygen measurement (80 μm above the cell layer). (c) An X-Z projection demonstrating the layering with the reconstructed liver acinus from confocal images of labeled hepatocytes, the LECM and HMVEC-D cells. The white scale bar is 10 μm.

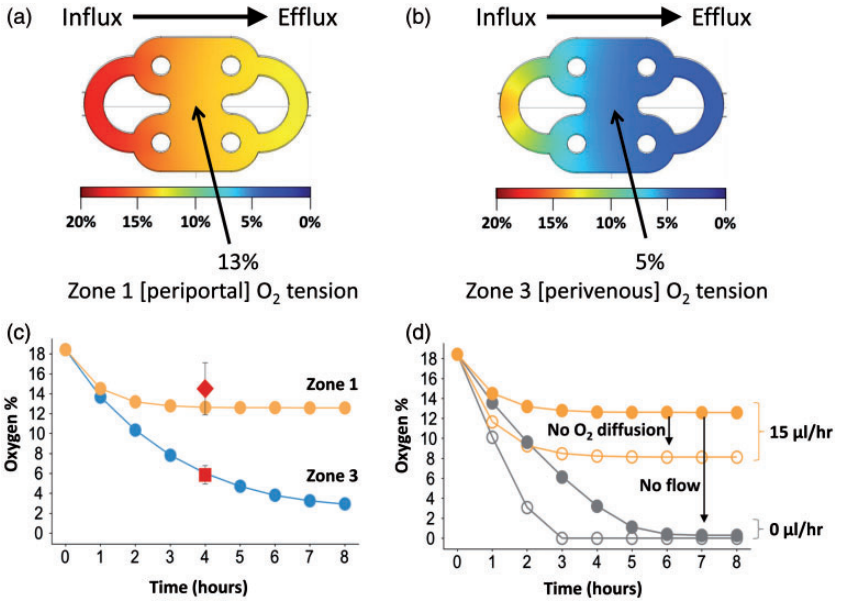

Figure 3 Computational simulations and experimental measurements of oxygen tension in the LAMPS model. (a) COMSOL simulation of oxygen tension in the LAMPS after 18 h at 15 µL/h (using 60,000 cells and OCR = 0.45 nmol/s/10^6 cells) predicts a gradient of oxygen from 12 to 14% in the main chamber of the module. (b) COMSOL simulation of oxygen tension in the LAMPS after 18 h at 5 µL/h (using 60,000 cells and OCR = 0.45 nmol/s/10^6 cells) predicts a gradient of oxygen from 4 to 6% in the main chamber of the module. (c) Comparison of experimentally measured oxygen tension with COMSOL simulations of oxygen tension in the LAMPS (OCR = 0.45 nmol/s/10^6 cells). COMSOL simulation results are plotted for flow rates of 15 µL/h (yellow) and 5 µL/h (blue) and 70,000 cells. Experimental oxygen measurements using ratiometric imaging (red markers, n = 3, error bars = ± 1 standard deviation) were taken 4 h after introducing media with RTDP and Alexa 488 dyes and maintaining a flow rate of 15 µL/h (♦) or 5 µL/h (■). (d) Comparison of the effects of flow and oxygen diffusion through PDMS on oxygen tension over time in a Nortis module (70,000 cells and an OCR = 0.45 nmol/s/10^6 cells). Simulations for flow rates of 15 µL/h (yellow) or 0 µL/h (gray) with oxygen influx through the PDMS (•) and without oxygen influx through the PDMS (○).

the number chosen for the computational model (data not shown), there can be some variability in cell density from device-to-device. Increasing the cell number in the simulation from 60,000 to 70,000 cells lowered the steady state oxygen level ~1.5% at 15 µL/h, and ~2.5% at 5 µL/h (Supplemental Figure S3(a)) but the difference in O_2 tension between the two flow rates remained about 8–10%. Because published values for hepatocyte OCR vary, and indeed may vary from lot-to-lot or species-to-species, we also examined the sensitivity of the model to OCR by running the simulation with OCR = 0.375, 0.40, 0.425 and 0.45 nmol/s/10^6 cells (Supplemental Figure S3(b)). Increasing OCR from 0.375 to 0.45 reduced the steady state oxygen level by about 2% at 15 µL/h and about 4% at 5 µL/h. Over this range of OCR values, the difference between the oxygen levels at 5 and 15 µL/h ranged from 6 to 8%. Although the diffusion of O_2 in PDMS has been well characterized, we wanted to evaluate the magnitude of the contribution of O_2 diffusion in PDMS to the final O_2 tension, and to explore what the O_2 tension would be in an O_2 impermeable plastic. In this same simulation, we further evaluate O_2 tension in the absence of flow, as when the flow is interrupted or the model is maintained in static state. To investigate these effects, simulations were carried out at 3 flow rates – 0, 5, and 15 µL/h, with and without oxygen diffusion though PDMS. The results of these simulations are shown in Figure 3(d). In the absence of O_2 diffusion in PDMS, the O_2 tension drops about 5% at 15 µL/h, and essentially to 0% in 3 h with no flow. In static conditions, the O_2 tension drops to near 0% in 3 h, with or without O_2 perfusion through PDMS, indicating that the OCR by the hepatocytes is much greater than the diffusivity through PDMS in this model.

The COMSOL simulations were used to evaluate the maximum shear stresses generated in the LAMPS. Differences in shear stress at flow rates of 5 and 15 µL/h might also contribute to observed differences in cellular functions. The COMSOL simulations indicated shear stress of 0.11 µPa, 0.34 µPa and 1.13 µPa at flow rates of 5, 15 and 50 µL/h, respectively. The shear stress in these experiments are more than three orders of magnitude below the "low" shear stresses of 1–33 mPa that were reported to have no significant effect on albumin or urea secretion by rat hepatocytes relative to controls.[22] In another study, Park *et al.*[55] demonstrated that "low" shear stresses of 23–50 mPa had no significant impact on hepatocyte viability.

Measuring O_2 tension in the LAMPS

The calibration and measurement of O_2, and the sensitivity to cell number predicted by the COMSOL model were initially tested in microplates (Supplemental Figure S4). The data show that the calibrated O_2 measurements using the ratiometric method described in materials and methods (Supplemental Figure S4(b)) and the COMSOL model (Supplemental Figure S4(c)) were in good agreement, and showed that at 30,000 cells/well the OCR by the hepatocytes on the bottom of the plates was sufficient to create an oxygen gradient axially in the microplate well. The oxygen tension was then calibrated and measured in the LAMPS after 4 h of flow at 5 and 15 µL/(red square and red

diamond in Figure 3(c)), for comparison with the COMSOL simulations. The results demonstrate that measurements taken at 5 and 15 μL/h agree with the simulations for 60–70,000 cells and an OCR of 0.45 nmol/s/10^6 cells.

Improvements to the cells and organization of the SQL-SAL model

Several modifications were made to the construction of the LAMPS (Table 1). The hepatocyte layer in the model was coated with a thin layer of porcine LECM to mimic the space of Disse, and provide an ECM surface on which the endothelial cells can attach, proliferate and form a protective layer. Figure 2(c) shows a cross-sectional image of the model showing that the layering of the hepatocytes, LECM and endothelial cells corresponds to the illustration in Figure 2(b).

To identify an improved endothelial cell line, three endothelial cell types were evaluated in co-culture with human primary hepatocytes: EA.Hy926 (the cell line used in SQL-SAL 1.0); TMNK-1 transformed liver endothelial cells; and HMVEC-D human dermal microvascular endothelial cells. Co-culture with HMVEC-D cells resulted in a steady increase in albumin secretion out to seven days and about twice as much albumin secretion as co-culture with EA.Hy926, whereas co-culture with TMNK-1 cells stimulated only about half as much albumin secretion as EA.Hy926 at seven days (Supplemental Figure S9(a)). Furthermore, co-culture with HMVEC-D cells resulted in a steady increase in urea secretion out to seven days and more than 1.5 times the secretion in the EA.Hy926 co-culture. Co-culture with TMNK-1 cells resulted in significantly lower urea secretion than EA.Hy926 (Supplemental Figure S9). These results demonstrate the significant interaction between the endothelial cells and the hepatocytes. Although liver endothelial cells (TMNK-1) might seem to be a better choice for the model based on their source, the HMVEC-D cells appear to provide a more physiological interaction with the hepatocytes, and therefore were chosen for use in the LAMPS. We continue to explore the use of primary liver-specific endothelial cells that will further improve the physiological value of the liver MPS.

Because immune mediated toxicity is an important mode of toxicity, having a functional Kupffer-like immune cell is an important component of the LAMPS model. Two different immune cells were evaluated in the LAMPS. The U-937 cells used in the SQL-SAL 1.0 were compared with THP-1, a monocytic cell line. When differentiated with TMA, and then exposed to 100 ng/mL LPS, the THP-1 cells were shown to release more than 10 times the amount of TNF-alpha as the U-937 cells (Supplemental Figure S10), and therefore were adopted in the LAMPS model.

Impact of oxygen zone-specific conditions on oxidative phosphorylation and glucose metabolism

Oxidative phosphorylation was measured indirectly as mitochondrial membrane potential, by labeling the mitochondria with TMRE (tetramethylrhodamine ethyl ester), a cell permeant red fluorescent dye that is sequestered in mitochondria in proportion to the intact membrane potential. Higher TMRE fluorescence indicates higher mitochondrial membrane potential, indicative of higher oxidative phosphorylation. Oxidative phosphorylation is known to be greater in Zone 1 than Zone 3 (Figure 1(c)). Three separate LAMPS devices at each flow rate (5 and 15 μL/h) were loaded overnight with media containing TMRE (100 nM). The next day, 12 fields were imaged in the central chamber of each device (see Figure S7), and the average TMRE fluorescence intensity in the stained area of the image was measured. The average intensity was normalized by the nuclear count for each device to eliminate cell density effects. TMRE intensity of the devices at 15 μL/h (Zone 1) was found to be significantly higher ($P \leq 0.05$) as compared to devices at flow rate of 5 μL/h (Zone 3) in agreement with expected zonation differences (Figure 4(a)). In parallel, efflux was also collected from each device to measure the amount of glucose remaining in the efflux media as an indication of the level of glycolysis. The amount of glucose remaining in the media was found to be significantly lower ($P \leq 0.05$) at 5 μL/h than 15 μL/h implying a higher level of glycolysis in Zone 3 (Figure 4(b)).

Impact of zonation on protein secretion and expression

Oxygen zonation in the liver effects protein secretions as well as expression of metabolic enzymes. To evaluate the capability of the LAMPS to recapitulate zonation dependent protein secretions, efflux media was collected and measured for albumin, urea and α1AT. Albumin synthesis from days 4 to 14 in the Zone 1 model was more than twice that observed in the Zone 3 model (Figure 5). Similarly, urea secretion from the Zone 1 model was approximately twice that in the Zone 3 model (Figure 5). In contrast, alpha-1 antitrypsin secretion was 5-fold higher in the Zone 3 model compared to the Zone

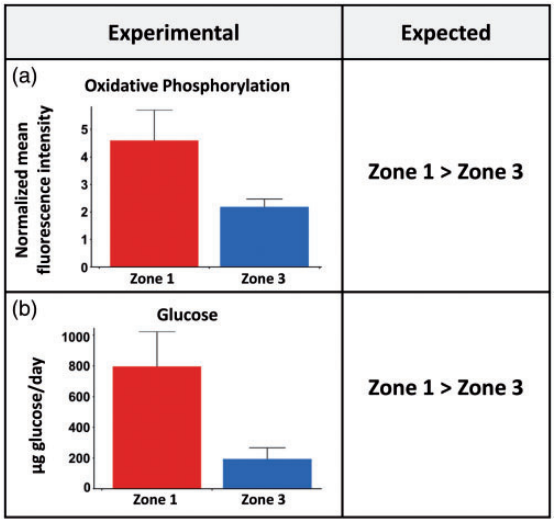

Figure 4 Comparison of oxidative phosphorylation and glycolysis in Zone 1 (15 μL/h) and Zone 3 (5 μL/h). Experimental column showed a good agreement with the expected zonation differences. (a) Comparison of average TMRE fluorescence normalized using total cell numbers to show higher mitochondrial membrane potential in Zone 1 as compared to Zone 3. (b) Glucose measurements in the media efflux from Zone 1 chips compared to Zone 3 chips indicate lower glucose in Zone 3 conditions, implying greater glycolysis in Zone 3. N = 3 and error bars represent standard deviation.

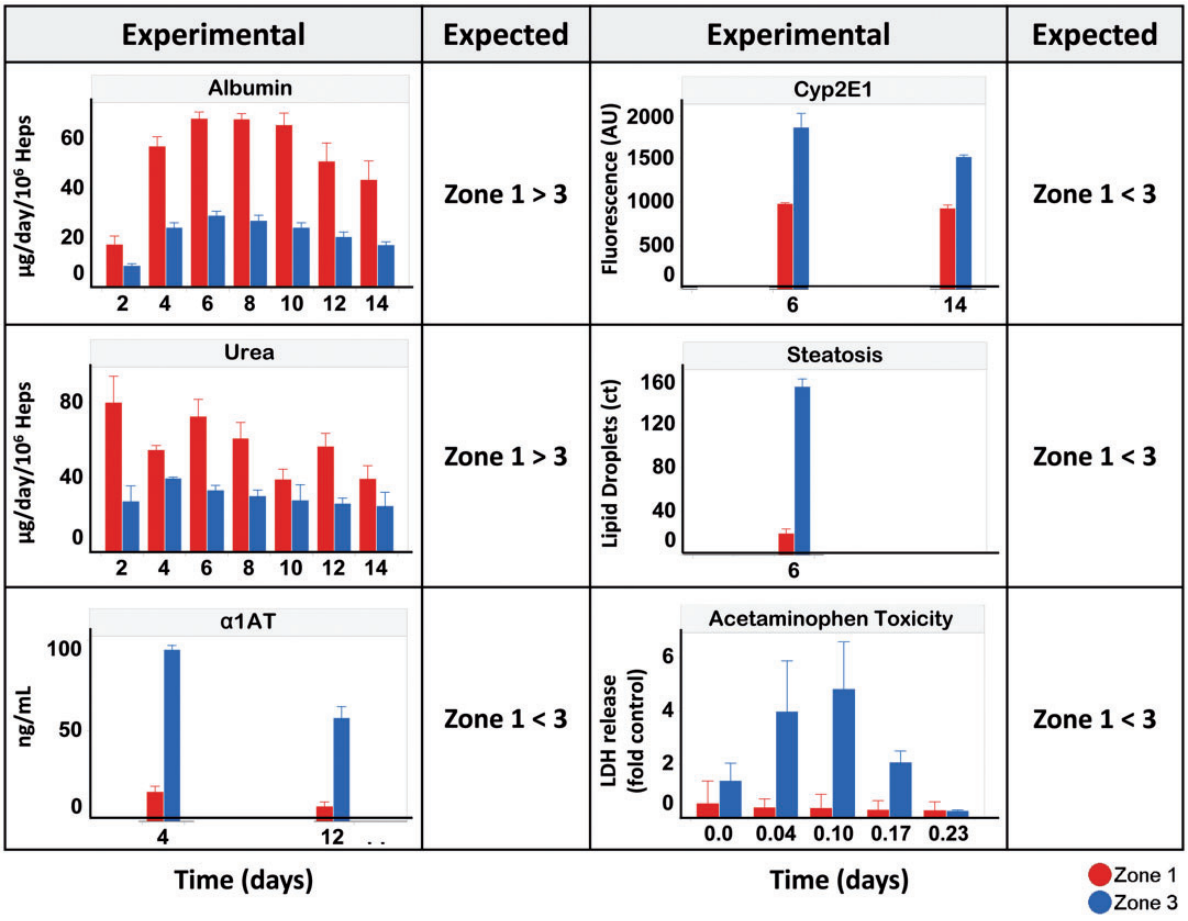

Figure 5 Comparison of the measured Experimental effects of Zone 3 (5 µL/h) vs. Zone 1 (15 µL/h) with the expected effects. Albumin, Urea, α1-antitrypsin (α1AT) secretion were measured in the efflux on the days indicated. Cytochrome P450, 2E1 (Cyp2E1) protein expression level was measured by imaging a fluorescent labeled antibody to Cyp2E1. Steatosis was measured by fluorescent imaging and counting lipid droplets. Acute acetaminophen toxicity was measured over 5.5 h as the ratio of LDH in the effluent to the average of control chips. All times are in days. N = 3 and error bars represent standard error for three replicates.

1 model (Figure 5). Taken together, these three secretion markers gave us confidence that the LAMPS models recapitulate *in vivo* zonation dependent physiology. As a further indication of zonation dependent physiology, immunohistochemistry labeling of cytochrome P450-CYP2E1 in the two models showed that expression level was uniform throughout the LAMPS, and was 1.5–2× higher in the Zone 3 model than in the Zone 1 model (Figure 5), consistent with *in vivo* physiology.[10]

Zonation dependent lipogenesis (steatosis)

Lipid storage in the liver is a highly dynamic and controlled process influenced by physiologic, hormonal and nutrient signals. The venous and arterial blood supply of hepatic blood produces structured environments that affect lipid zonation. In this study, hepatocytes under a lower oxygen concentration (Zone 3 model) displayed a 6× higher number of lipid filled cells compared to the Zone 1 model (Figure 5), consistent with characteristics observed in the human liver,[13] in which liver histology specimens displayed numerous large lipid droplets most prominent in hepatocytes surrounding the central vein (Zone 3).

Impact of zonation on acetaminophen toxicity

Acetaminophen hepatotoxicity is dependent on the increased expression of Cyp2E1 found in the Zone 3 perivenous human hepatocytes[56] and also demonstrated in the Zone 3 LAMPS (Figure 5). While devices were maintained at 5 and 15 µL/h for five days for zone conditioning, acute drug exposure was carried out at the same flow rate (10 µL/h) to standardize the exposure to the drug. The Zone 3 conditioned devices displayed a significant increase in LDH release (maximum of ~10-fold) compared to the Zone 1 conditioned devices, consistent with human studies showing acetaminophen toxicity occurs primarily in Zone 3.[56]

Discussion

Next generation LAMPS

Here we describe an improved version of the human liver MPS (LAMPS). This next generation liver MPS better recreates the structural organization and physiology of the human liver sinusoid, through improvements in three main areas: (1) 3D structure/matrix; (2) improved cellular functions; and (3) control of oxygenation (specific zones established in single MPS). The improved layering of the

cells and the inclusion of the porcine LECM layer to mimic the Space of Disse, provides a surface on which the endothelial cells can proliferate to form a barrier layer isolating the hepatocytes from flow and to better model the *in vivo* relationship between hepatocytes and endothelial cells. LAMPS also has improved endothelial and Kupffer-like immune cells. Because we were using four different cell types in this MPS, we also used an improved perfusion media consisting of HMM plus FBS, VEGF and LECM which supported the growth and health of both hepatocytes and NPCs. The improved architecture and new nonparenchymal cell types and media were shown to enhance albumin and urea secretions and the more robust release of TNF-alpha in response to LPS. However, a more universal media with less glucose and dexamethasone that supports all liver functions is still under development.[57]

LAMPS also offers a unique approach to controlling oxygenation, using computational modeling to optimize oxygen flows and experimental methods to measure oxygen in the models. As a result, LAMPS models were shown to recreate liver Zones 1 and 3 oxygen microenvironments in separate devices and multiple physiological functions known to be associated with those microenvironments. The oxygen tensions achieved in the LAMPS closely mimic oxygenation in the *in vivo* liver. The ability to stimulate specific zonation functions in cryopreserved primary human hepatocytes supports the perspective that these cells are relatively ''plastic'' and can be induced to function differently under different microenvironmental conditions.[58] Taken together, the improvements in the LAMPS were shown to model zonation-specific functions including albumin synthesis, nitrogen metabolism and cytochrome P450 (CYP) activity,[40] and are expected to lead to a better understanding of liver physiological functions in the toxic response as well as for modeling liver diseases.

Other liver model systems have used cell–cell interactions, cell–matrix interactions, modifications to cell media, or scaffolds to promote the maintenance of liver cell viability and function.[4] Previous studies have shown that biomaterials such as porcine LECM retain numerous molecular constituents including cell adhesion proteins and immobilized growth factors found in the native tissue.[59] In LAMPS, we improved the structural organization of the model by depositing a thin layer of porcine LECM between the hepatocytes and endothelial cells, to mimic the space of Disse (Figure 2). The Space of Disse is a less than 1 μm layer between the hepatocytes and the liver sinusoidal endothelial cells (LSEC) that protect the hepatocytes from the shear generated by the blood flow.[60] The endothelial cells in the liver help to exchange some mid and small size molecules between the hepatocytes and the blood stream. The complex composition of proteins in the porcine LECM used here should better resemble the human LECM, sharing the composition of collagen, fibronectin and laminin that helps to mimic the human liver microenvironment. Other methods have been used to artificially mimic the space of Disse, including an ultrathin collagen layer[61] and the use of polyelectrolyte multilayers of chitosan-hyaluronic acid.[62] However, it is well established that LECM also has growth factors which regulate hepatocyte function.[40] Furthermore, it has been shown that sinusoidal endothelial cells cultured in LECM maintain their phenotype for a longer period of time due to microenvironmental factors.[63] We are currently testing LSECs for the next generation liver MPS that will also have a vascular unit.

Measuring oxygen tension in LAMPS

Oxygen measurements in microfluidic devices typically have relied on the use of fluorescent probes that are quenched by oxygen, such as ruthenium dyes or platinum/palladium porphyrin dyes. Such dyes can be incorporated into the media and flowed through the devices,[64–66] patterned as spots or thin films that are integrated into the device at the time of fabrication,[29,67–69] or as particles or beads that are introduced into the device after assembly.[70–72] In this study, we used a solution of RTDP in media in order to measure oxygen temporally and spatially throughout the LAMPS volume. Although RTDP concentrations higher than 0.2 mM were reported to be phototoxic, lower concentrations were found to be cell compatible.[73] RTDP was first used for intra-cellular measurements, since it is taken up by cells over time.[74] This is a drawback when being used for extracellular oxygen measurements, as it was here, since it limits the amount of time the MPS system can be exposed to RTDP prior to the measurement, and therefore limits long-term continuous oxygen monitoring. Because of this limitation, some recent work has used RTDP to characterize oxygen concentrations in cell free channels and then culture cells with no dye;[75–77] however, this has the disadvantage that the impact of cellular oxygen consumption is not taken into account. In the LAMPS model, oxygen consumption has a significant effect on the steady state oxygen tension (Supplemental Figure S3). Polymers or beads with integral or attached fluorescent oxygen probes should avoid the cellular uptake issue and can be distributed spatially within the MPS. Beads are an attractive alternative to dye solutions and we are currently evaluating commercial options and synthesized versions.

Quenching of fluorescence can be measured either by fluorescence intensity or fluorescent lifetime. Fluorescence intensity measurements can be made with essentially any fluorescence microscope imaging system, but as an extensive property that depends on the path length and dye concentration, a normalization is required, such as by ratio imaging as presented here.[46] Fluorescence lifetime avoids volume and concentration effects, and is therefore often used. However, fluorescence lifetime requires more specialized equipment, not found in most labs. In this study, we demonstrated the calibration of an established oxygen sensitive fluorescent dye, RTDP, through ratio imaging with Alexa 488. RTDP and Alexa 488 are both soluble in media and can be flowed throughout an MPS system, allowing spatial and temporal measurements of oxygen. This approach is generally applicable to microfluidic systems that are amenable to imaging.

Characterization and control of zonation

Relatively, few MPS studies have addressed measuring, modeling and controlling oxygenation in microfluidic

systems. As a result, the oxygen levels in many organ MPS with the potential impact of oxygen tension on cell health and function are not known. Variation in oxygen tension has been shown to impact oxygen consumption, metabolic functions, protein synthesis, and gene expression. It is therefore imperative to measure and to control the oxygen level in MPS. The human primary hepatocytes used in this study have a relatively high oxygen consumption rate, ranging from 0.3 to 0.9 nmol/s/10^6 cells, due to their high number of mitochondria.[78] For reference, HepG2 cells consume 10-fold less oxygen.[79,80] It is clear from Figure 3(d) that in this model, both media flow and PDMS permeability play important roles in regulating oxygen. It is also clear that PDMS permeability alone does not provide adequate oxygenation of the cells, and that without PDMS permeability, such as in an oxygen impermeable plastic device, much higher flow rates would be required to maintain the oxygen tension in the model. These results suggest that analysis of oxygenation of microfluidic cellular models should be an integral element of the design of MPS, and also measured in the device under normal operating conditions. The sensitivity of the oxygen tension to media flow rate in the LAMPS turned out to be an advantage, allowing simulation of liver Zones 1 and 3 with a relatively small variation in flow rate in the very low shear domain from 15 μL/h to 5 μL/h, respectively. Because we were able to create distinct Zones in individual devices, this MPS can also be used to investigate zone-specific diseases and toxicology.[6,81]

Regulating oxygen levels by slightly varying the flow rate is easily accomplished and requires no additional equipment or materials. However, this method only works in microfluidic systems with the right balance of OCR, material permeability and media flow rate. While hepatocytes have a relatively high OCR, requiring more oxygen influx, control of oxygen by modulating the media flow rate for other cell types with lower OCR may also be possible, but may require a greater variation in flow rate.

The drawback to using flow for oxygen control is that the effects of oxygen might be confounded by shear stress, variation in transport of other media components, and removal of cellular secretions and waste products.[22,82] Shear forces have been shown to effect albumin and urea secretions, CyP450 activities, cell morphology and viability and likely impact other functions.[83–85] Shear forces near the hepatocyte layer were calculated using COMSOL, and at flow rates of 5 and 15 μl/h, the shear stresses were 0.11 μPa and 0.34 μPa, respectively. Tilles *et al*.[22] examined the effects of shear stress using rat hepatocytes co-cultured with 3T3-J2 fibroblasts in a microchannel flat plate bioreactor. After three days of flow, they found that ''lower'' wall shear stresses (1–33 mPa) resulted in a 2.6-fold and 1.9-fold higher albumin and urea secretion, respectively, compared to higher shear stresses (500–2100 mPa). More importantly, within the range of ''lower'' shear stresses tested (1, 7, 18 and 33 mPa), there were no significant differences in albumin or urea synthesis. This indicates that over a 33-fold range in shear stress from 1 to 33 mPa, there is no significant impact on the hepatocytes secretion of albumin and urea. Park *et al*.[55] demonstrated that after 36 h of perfusion at ''lower'' shear stresses (23–50 mPa), hepatocyte viability was >94%, while higher shear stresses (101 mPa and 504 mPa) reduced the viability to 28% and 0%, respectively. Thus, primary hepatocyte function and viability are clearly affected by shear stresses greater than, or approximately equal to 100 mPa.

In contrast, the shear stresses generated in the LAMPS are more than three orders of magnitude lower than the ''low'' shear stresses that were shown in the studies cited above to have no significant effect on albumin, urea or viability. Furthermore, the 3-fold range of flow rates used in this study is very small relative to the 33-fold range evaluated by Tilles *et al*.[22] which resulted in no significant variation in albumin or urea production. Considering that the measured responses, including increases in α1AT, Cyp2E1, steatosis and acetaminophen toxicity in Zone 3 (lower shear) and the decrease in albumin and urea in Zone 3 (lower shear) are consistent with what is known about the effect of oxygen zonation on cellular functions, the zonation effects observed in the LAMPS are unlikely to result from the difference in shear stress between the two models. However, although there is no evidence that primary hepatocytes are sensitive to the low shear forces in the LAMPS model, stem cell-derived hepatocytes may be more sensitive to shear. In one study, it was shown in 2D cultures of human embryonic stem cell-derived hepatocyte like cells (HLCs), that Cyp1A2 activity increased 4-fold from near the static activity, when the shear force was increased from 2.9 μPa to 4.7 μPa.[85] In 3D culture, however, both shear forces led to about a 7-fold reduction in Cyp1A2 activity relative to control.

Implications of oxygen tension in other organ MPS and device materials

All organ MPS require appropriate physiological oxygen levels in order to accurately mimic organ level metabolism. This becomes a major challenge as the focus moves towards interconnecting organs each with their own oxygen requirements. Oxygen-dependent metabolism is well known in the liver, but some organs such as the lungs and brain require higher or lower oxygen tensions,[86] while others operate under a gradient. Conventional approaches to organ MPS however rarely characterize or control the oxygen levels available to cells. This can be attributed to the complexity of such systems – with multiple cell types and fluidic channels, and to the difficulty in measuring oxygen levels with precision at regions of interest. PDMS, a common material for fabricating microfluidic devices, is oxygen permeable. However, the thickness of the PDMS layer and distance between PDMS boundary and cell layer (thickness of flow channel) can greatly slow the flux of oxygen to the cell layers. The use of oxygen impermeable plastic devices makes it even more crucial to define the oxygen levels in these devices for normoxic function. Too low a flow rate can create a hypoxic environment, while higher flow rates can result in a hyperoxic environment and shear stress induced damage, both of which are detrimental to the physiology.

Demonstration of zonation dependent physiology in the LAMPS

The Zone 1 and Zone 3 LAMPS models successfully demonstrated zonation dependent physiology of oxidative phosphorylation, glycolysis, albumin, urea and α1AT secretion, Cyp2E1 expression, steatosis, and acetaminophen toxicity that were consistent with known *in vivo* physiology. In the Zone 1 LAMPS model, albumin and urea secretion out to 15 days were significantly higher than the SQL-SAL 1.0, while the Zone 3 LAMPS model was only slightly higher (Figure 5 vs. Figure 3 in Vernetti, Senutovitch[17]). This is consistent with the operation of the SQL-SAL 1.0 at 5 μL/h, like the Zone 3 LAMPS, suggesting that SQL-SAL 1.0 may have been more like the Zone 3 model, again emphasizing the importance of measuring oxygen tension in microfluidic organ models, even though the PDMS construction provides oxygen permeability. The consistency of zonation dependent physiology over the broad range of markers assayed in this study gives a high degree of confidence that the LAMPS can reliably recreate zonal physiology.

Although acetaminophen hepatotoxicity has been well known and well-studied for five decades it continues to account for 50% of drug-induced acute liver failure and nearly 20% of the liver transplant cases from accidental and intentional overdosing.[87] Anundi and Lahteenmaki[88] first reported acetaminophen toxicity was dependent on the increased expression of Cyp2E1 found in the Zone 3 perivenous hepatocytes. In the LAMPS, we found almost twice the expression of Cyp2E1 in Zone 3 vs. Zone 1 (Figure 5). Following high level of acetaminophen ingestion enough of the reactive metabolite, N-acetyl-p-benzoquinone imine (NAPQI) from CYP2E1 (with minor contributions from Cyp 1A2 and Cyp 3A4) metabolism exhausts protective GSH in the hepatocytes. Although the molecular target of NAPQI is not known, most research agrees NAPQI covalent binding to mitochondrial and other proteins is most likely the cause of hepatocellular death.[89,90] Acetaminophen was chosen as the model toxin to confirm preferential Zone 3 toxicity in the LAMPS zonation model.

In summary, the LAMPS is robust and easy to assemble and to operate. It recapitulates liver acinus structure and multiple zone-specific functions. In its current form, the LAMPS is most amenable to low throughput, acute through chronic studies, including liver disease models, evaluating the effects of varying concentrations of hormones or other regulators, prioritizing compounds for preclinical studies, optimizing chemistry in structure activity relationship (SAR) projects, as well as in rising dose studies for initial dose ranging.

Future prospects

The performance of the LAMPS model in simulating Zone 1 and 3 physiology demonstrates that it will be a valuable model for drug safety and disease modeling. Human zone-specific physiology, toxicology and disease modeling can now be explored in detail over time. A limitation of the model as described here is that Zone 3 is not downstream from Zone 1, as it would be *in vivo.* Results indicate that the functional differences measured here were consistent with what is known about zonation effects, despite the standalone Zone 3 model. Perhaps some differences in the magnitude of these functional differences, or differences in other functions would be observed in a more physiological arrangement. One experimental approach to addressing this question is to couple Zone 1 and Zone 3 LAMPS, which will require modulating the flow rate between Zone 1 and Zone 3, or an alternative approach to creating zonation in the model.

Further optimization of the liver MPS includes development of an all induced pluripotent stem cell (iPSC) version for personalized toxicity and disease modeling combined with a more general physiological media that supports hepatocyte and non-parenchymal cell functions. Although using primary human NPCs in the LAMPS might have provided a better model of the human liver, we chose to use cell lines for the reliability and reproducibility at this time. We will be using all human primary cells in future experiments, followed by the introduction of iPSCs. In addition, a vascularized liver MPS is important to allow physiologically relevant flow within the ''sinusoid,'' coupled with a distinct and lower interstitial flow in a 2-chamber design. The vascularized liver MPS in development should allow the creation of zonation within a single liver MPS, as well as allowing more physiologically relevant coupling in multi-organ MPS.

Authors' contributions: All authors participated in the study design, analysis of the data, interpretation of the results and review of the manuscript; FTL-M, SMG, ADS, JW and RD conducted the experiments, AHG, SMG, FTL-M, ADS and DLT wrote the manuscript.

ACKNOWLEDGEMENTS

We would like to acknowledge the technical assistance with LC-MS data acquisition from Patrick Oberly (UPitt) and Margaret Minnigh (UPitt) and also technical help from David Zaidins (UPitt). We thank Michelle Scarritt in the lab of Stephen Badylak (UPitt) for supplying us with porcine liver extracellular matrix and valuable discussions. We also wish to acknowledge the ongoing collaborations and discussions with Drs. Paul Monga and Alex Soto-Gutierrez in liver physiology, diseases and production of human liver iPSCs. Dr. Lance Davidson kindly permitted us to use his confocal microscope. Research reported in this publication was supported by the National Institutes of Health/National Center for Advancing Translational Sciences (NIH/NCATS) under awards UH3TR000503 and NIH P30 CA047904, as well as the U.S. Environmental Protection Agency (EPA) STAR 8357360. Research reported in this publication made use of instrumentation funded by the National Institutes Of Health Award Number S10OD012269.

DECLARATION OF CONFLICTING INTERESTS

The author(s) declared no potential conflicts of interest with respect to the research, authorship, and/or publication of this article.

REFERENCES

1. Lamers WH, Hilberts A, Furt E, Smith J, Jonges GN, van Noorden CJ, Janzen JWG, Charles R, Moorman AF. Hepatic enzymic zonation: A reevaluation of the concept of the liver acinus. *Hepatology* 1989;**10**: 72–6
2. Jungermann K, Kietzmann T. Zonation of parenchymal and nonparenchymal metabolism in liver. *Ann Rev Nutr* 1996;**16**:179–203
3. Frevert U, Engelmann S, Zougbede S, Stange J, Ng B, Matuschewski K, Liebes L, Yee H. Intravital observation of Plasmodium berghei sporozoite infection of the liver. *PLoS Biol* 2005;**3**:e192
4. Godoy P, Hewitt N, Albrecht U, Andersen M, Ansari N, Bhattacharya S, Bode J, Bolleyn J, Borner C, Böttger J, Braeuning A, Budinsky R, Burkhardt B, Cameron N, Camussi G, Cho C-S, Choi Y-J, Craig Rowlands J, Dahmen U, Damm G, Dirsch O, Donato M, Dong J, Dooley S, Drasdo D, Eakins R, Ferreira K, Fonsato V, Fraczek J, Gebhardt R, Gibson A, Glanemann M, Goldring CP, Gómez-Lechón M, Groothuis GM, Gustavsson L, Guyot C, Hallifax D, Hammad S, Hayward A, Häussinger D, Hellerbrand C, Hewitt P, Hoehme S, Holzhütter H-G, Houston JB, Hrach J, Ito K, Jaeschke H, Keitel V, Kelm J, Kevin Park B, Kordes C, Kullak-Ublick G, LeCluyse E, Lu P, Luebke-Wheeler J, Lutz A, Maltman D, Matz-Soja M, McMullen P, Merfort I, Messner S, Meyer C, Mwinyi J, Naisbitt D, Nussler A, Olinga P, Pampaloni F, Pi J, Pluta L, Przyborski S, Ramachandran A, Rogiers V, Rowe C, Schelcher C, Schmich K, Schwarz M, Singh B, Stelzer EK, Stieger B, Stöber R, Sugiyama Y, Tetta C, Thasler W, Vanhaecke T, Vinken M, Weiss T, Widera A, Woods C, Xu J, Yarborough K, Hengstler J. Recent advances in 2D and 3D in vitro systems using primary hepatocytes, alternative hepatocyte sources and non-parenchymal liver cells and their use in investigating mechanisms of hepatotoxicity, cell signaling and ADME. *Arch Toxicol* 2013;**87**:1315–530
5. Gebhardt R, Matz-Soja M. Liver zonation: Novel aspects of its regulation and its impact on homeostasis. *World J Gastroenterol* 2014;**20**:8491–504
6. Soto-Gutierrez A, Gough A, Vernetti LA, Taylor DL, Monga SP. Pre-clinical and clinical investigations of metabolic zonation in liver diseases: The potential of microphysiology systems. *Exp Biol Med* 2017;**242**:1605–16
7. Colombo C. Liver disease in cystic fibrosis. *Curr Opin Pulmon Med* 2007;**13**:529–36
8. Burke ZD, Tosh D. The Wnt/beta-catenin pathway: Master regulator of liver zonation? *BioEssays* 2006;**28**:1072–7
9. Monga SP. beta-catenin signaling and roles in liver homeostasis, injury, and tumorigenesis. *Gastroenterology* 2015;**148**:1294–310
10. Colnot S, Perret C. Liver zonation. In: Monga SSP (ed.). *Molecular pathology of liver diseases*. Boston, MA: Springer, 2011, pp. 7–16
11. Tao J, Xu E, Zhao Y, Singh S, Li X, Couchy G, Chen X, Zucman-Rossi J, Chikina M, Monga SP. Modeling a human HCC Subset in mice through co-expression of met and point-mutant beta-catenin. *Hepatology* 2016; **64**:1587–1605
12. Moreau M, Riviere B, Vegna S, Aoun M, Gard C, Ramos J, Assenat E, Hibner U. Hepatitis C viral proteins perturb metabolic liver zonation. *J Hepatol* 2015;**62**:278–85
13. Wattacheril J, Seeley EH, Angel P, Chen H, Bowen BP, Lanciault C, Caprioli RM, Abumrad N, Flynn CR. Differential intrahepatic phospholipid zonation in simple steatosis and nonalcoholic steatohepatitis. *PloS One* 2013;**8**:e57165
14. Huh D, Torisawa YS, Hamilton GA, Kim HJ, Ingber DE. Microengineered physiological biomimicry: Organs-on-chips. *Lab Chip* 2012;**12**:2156–64
15. Huh D, Hamilton GA, Ingber DE. From 3D cell culture to organs-on-chips. *Trends Cell Biol* 2011;**21**:745–54
16. Bhatia SN, Ingber DE. Microfluidic organs-on-chips. *Nat Biotechnol* 2014;**32**: 760–72
17. Vernetti LA, Senutovitch N, Boltz R, DeBiasio R, Ying Shun T, Gough A, Taylor DL. A human liver microphysiology platform for investigating physiology, drug safety, and disease models. *Exp Biol Med* 2016;**241**:101–14
18. Nakao Y, Kimura H, Sakai Y, Fujii T. Bile canaliculi formation by aligning rat primary hepatocytes in a microfluidic device. *Biomicrofluidics* 2011;**5**: 22212
19. Lee PJ, Hung PJ, Lee LP. An artificial liver sinusoid with a microfluidic endothelial-like barrier for primary hepatocyte culture. *Biotechnol Bioeng* 2007;**97**:1340–6
20. Carraro A, Hsu WM, Kulig KM, Cheung WS, Miller ML, Weinberg EJ, Swart EF, Kaazempur-Mofrad M, Borenstein JT, Vacanti JP, Neville C. In vitro analysis of a hepatic device with intrinsic microvascular-based channels. *Biomed Microdev* 2008;**10**:795–805
21. Leclerc E, Sakai Y, Fujii T. Microfluidic PDMS (polydimethylsiloxane) bioreactor for large-scale culture of hepatocytes. *Biotechnol Progr* 2004;**20**:750–5
22. Tilles AW, Baskaran H, Roy P, Yarmush ML, Toner M. Effects of oxygenation and flow on the viability and function of rat hepatocytes cocultured in a microchannel flat-plate bioreactor. *Biotechnol Bioeng* 2001;**73**:379–89
23. Allen JW, Khetani SR, Bhatia SN. In vitro zonation and toxicity in a hepatocyte bioreactor. *Toxicol Sci* 2005;**84**:110–9
24. Allen JW, Bhatia SN. Formation of steady-state oxygen gradients in vitro: Application to liver zonation. *Biotechnol Bioeng* 2003;**82**:253–62
25. Sato A, Kadokura K, Uchida H, Tsukada K. An in vitro hepatic zonation model with a continuous oxygen gradient in a microdevice. *Biochem Biophys Res Commun* 2014;**453**:767–71
26. Vernetti L, Gough A, Baetz N, Blutt S, Broughman JR, Brown JA, Foulke-Abel J, Hasan N, In J, Kelly E, Kovbasnjuk O, Repper J, Senutovitch N, Stabb J, Yeung C, Zachos NC, Donowitz M, Estes M, Himmelfarb J, Truskey G, Wikswo JP, Taylor DL. Functional coupling of human microphysiology systems: Intestine, liver, kidney proximal tubule, blood-brain barrier and skeletal muscle. *Scientific Reports* 2017;**7**:42296
27. Markov DA, Lillie EM, Garbett SP, McCawley LJ. Variation in diffusion of gases through PDMS due to plasma surface treatment and storage conditions. *Biomed Microdev* 2014;**16**:91–6
28. Toepke MW, Beebe DJ. PDMS absorption of small molecules and consequences in microfluidic applications. *Lab Chip* 2006;**6**:1484–6
29. Ochs CJ, Kasuya J, Pavesi A, Kamm RD. Oxygen levels in thermoplastic microfluidic devices during cell culture. *Lab Chip* 2014;**14**:459–62
30. Wisse E, De Zanger RB, Charels K, Van Der Smissen P, McCuskey RS. The liver sieve: Considerations concerning the structure and function of endothelial fenestrae, the sinusoidal wall and the space of Disse. *Hepatology* 1985;**5**:683–92
31. Arias IM, Boyer JL, Chisari FV, Fausto M, Schachter D, Sharftx DA. *The liver: Biology and pathobiology*, 4th ed. Philadelphia, PA: Lippincott Williams and Wilkins, 2001:1628
32. Brenner DA. Molecular pathogenesis of liver fibrosis. *Trans Am Clin Climatol Assoc* 2009;**120**:361–8
33. Orrego H, Medline A, Blendis LM, Rankin JG, Kreaden DA. Collagenisation of the Disse space in alcoholic liver disease. *Gut* 1979;**20**:673–9
34. Xu L, Hui AY, Albanis E, Arthur MJ, O'Byrne SM, Blaner WS, Mukherjee P, Friedman SL, Eng FJ. Human hepatic stellate cell lines, LX-1 and LX-2: New tools for analysis of hepatic fibrosis. *Gut* 2005;**54**:142–51
35. Bonner JC. Regulation of PDGF and its receptors in fibrotic diseases. *Cytokine Growth Factor Rev* 2004;**15**:255–73
36. Naciri M, Kuystermans D, Al-Rubeai M. Monitoring pH and dissolved oxygen in mammalian cell culture using optical sensors. *Cytotechnology* 2008;**57**:245–50
37. Newby D, Marks L, Lyall F. Dissolved oxygen concentration in culture medium: Assumptions and pitfalls. *Placenta* 2005;**26**:353–7
38. Kostadinova R, Boess F, Applegate D, Suter L, Weiser T, Singer T, Naughton B, Roth A. A long-term three dimensional liver co-culture system for improved prediction of clinically relevant drug-induced hepatotoxicity. *Toxicol Appl Pharmacol* 2013;**268**:1–16
39. Jang C-H, Choi J-H, Byun M-S, Jue D-M. Chloroquine inhibits production of TNF-α, IL-1β and IL-6 from lipopolysaccharide-stimulated human monocytes/macrophages by different modes. *Rheumatology* 2006;**45**:703–10

40. Loneker AE, Faulk DM, Hussey GS, D'Amore A, Badylak SF. Solubilized liver extracellular matrix maintains primary rat hepatocyte phenotype in-vitro. *J Biomed Mater Res Part A* 2016;**104**:957–65
41. Senutovitch N, Vernetti L, Boltz R, DeBiasio R, Gough A, Taylor DL. Fluorescent protein biosensors applied to microphysiological systems. *Exp Biol Med* 2015;**240**:795–808
42. Giulitti S, Magrofuoco E, Prevedello L, Elvassore N. Optimal periodic perfusion strategy for robust long-term microfluidic cell culture. *Lab Chip* 2013;**13**:4430–41
43. Buck LD, Inman SW, Rusyn I, Griffith LG. Co-regulation of primary mouse hepatocyte viability and function by oxygen and matrix. *Biotechnol Bioeng* 2014;**111**:1018–27
44. Kidambi S, Yarmush RS, Novik E, Chao P, Yarmush ML, Nahmias Y. Oxygen-mediated enhancement of primary hepatocyte metabolism, functional polarization, gene expression, and drug clearance. *Proc Natl Acad Sci* 2009;**106**:15714–9
45. Balis UJ, Behnia K, Dwarakanath B, Bhatia SN, Sullivan SJ, Yarmush ML, Toner M. Oxygen consumption characteristics of porcine hepatocytes. *Metab Eng* 1999;**1**:49–62
46. Bright GR, Fisher GW, Rogowska J, Taylor DL. Fluorescence ratio imaging microscopy. *Meth Cell Biol* 1989;**30**:157–92
47. Chen YA, King AD, Shih HC, Peng CC, Wu CY, Liao WH, Tung YC. Generation of oxygen gradients in microfluidic devices for cell culture using spatially confined chemical reactions. *Lab Chip* 2011;**11**:3626–33
48. Schindelin J, Arganda-Carreras I, Frise E, Kaynig V, Longair M, Pietzsch T, Preibisch S, Rueden C, Saalfeld S, Schmid B, Tinevez J-Y, White DJ, Hartenstein V, Eliceiri K, Tomancak P, Cardona A. Fiji: An open-source platform for biological-image analysis. *Nat Meth* 2012;**9**:676–82
49. Nilsen EM, Johansen F-E, Jahnsen FL, Lundin KEA, Scholz T, Brandtzaeg P, Haraldsen G. Cytokine profiles of cultured microvascular endothelial cells from the human intestine. *Gut* 1998;**42**:635–42
50. Unger RE, Krump-Konvalinkova V, Peters K, Kirkpatrick CJ. In vitro expression of the endothelial phenotype: Comparative study of primary isolated cells and cell lines, including the novel cell line HPMEC-ST1.6R. *Microvasc Res* 2002;**64**:384–97
51. Bouïs D, Hospers GAP, Meijer C, Molema G, Mulder NH. Endothelium in vitro: A review of human vascular endothelial cell lines for blood vessel-related research. *Angiogenesis* 2001;**4**:91–102
52. Park EK, Jung HS, Yang HI, Yoo MC, Kim C, Kim KS. Optimized THP-1 differentiation is required for the detection of responses to weak stimuli. *Inflamm Res* 2007;**56**:45–50
53. Cho CH, Park J, Nagrath D, Tilles AW, Berthiaume F, Toner M, Yarmush ML. Oxygen uptake rates and liver-specific functions of hepatocyte and 3T3 fibroblast co-cultures. *Biotechnol Bioeng* 2007;**97**:188–99
54. Wagner BA, Venkataraman S, Buettner GR. The rate of oxygen utilization by cells. *Free Rad Biol Med* 2011;**51**:700–12
55. Park J, Li Y, Berthiaume F, Toner M, Yarmush ML, Tilles AW. Radial flow hepatocyte bioreactor using stacked microfabricated grooved substrates. *Biotechnol Bioeng* 2008;**99**:455–67
56. McGill MR, Sharpe MR, Williams CD, Taha M, Curry SC, Jaeschke H. The mechanism underlying acetaminophen-induced hepatotoxicity in humans and mice involves mitochondrial damage and nuclear DNA fragmentation. *J Clin Invest* 2012;**122**:1574–83
57. Clark A, Bo M, Taylor DL, Griffith L, Wells A. Liver metastasis: Microenvironments and ex-vivo models. *Exp Biol Med* 2016;**241**:1639–52
58. Talamini MA, Kappus B, Hubbard A. Repolarization of hepatocytes in culture. *Hepatology* 1997;**25**:167–72
59. Voytik-Harbin SL, Brightman AO, Kraine MR, Waisner B, Badylak SF. Identification of extractable growth factors from small intestinal submucosa. *J Cell Biochem* 1997;**67**:478–91
60. Kuntz E, Kuntz H-D. *Hepatology, principles and practice: History, morphology, biochemistry, diagnostics, clinic, therapy*. Heidelberg: Springer Science & Business Media, 2006
61. McCarty WJ, Usta OB, Luitje M, Bale SS, Bhushan A, Hegde M, Golberg I, Jindal R, Yarmush ML. A novel ultrathin collagen nanolayer assembly for 3-D microtissue engineering: Layer-by-layer collagen deposition for long-term stable microfluidic hepatocyte culture. *Technology* 2014;**2**:67–74
62. Kim Y, Larkin AL, Davis RM, Rajagopalan P. The design of in vitro liver sinusoid mimics using chitosan-hyaluronic acid polyelectrolyte multilayers. *Tissue Eng Part A* 2010;**16**:2731–41
63. March S, Hui EE, Underhill GH, Khetani S, Bhatia SN. Microenvironmental regulation of the sinusoidal endothelial cell phenotype in vitro. *Hepatology* 2009;**50**:920–8
64. Sud D, Mehta G, Mehta K, Linderman J, Takayama S, Mycek MA. Optical imaging in microfluidic bioreactors enables oxygen monitoring for continuous cell culture. *J Biomed Opt* 2006;**11**:050504
65. Mehta G, Mehta K, Sud D, Song JW, Bersano-Begey T, Futai N, Heo YS, Mycek MA, Linderman JJ, Takayama S. Quantitative measurement and control of oxygen levels in microfluidic poly(dimethylsiloxane) bioreactors during cell culture. *Biomed Microdev* 2007;**9**:123–34
66. Peng CC, Liao WH, Chen YH, Wu CY, Tung YC. A microfluidic cell culture array with various oxygen tensions. *Lab Chip* 2013;**13**:3239–45
67. Molter TW, McQuaide SC, Suchorolski MT, Strovas TJ, Burgess LW, Meldrum DR, Lidstrom ME. A microwell array device capable of measuring single-cell oxygen consumption rates. *Sens Actuators B Chem* 2009;**135**:678–86
68. Ungerbock B, Charwat V, Ertl P, Mayr T. Microfluidic oxygen imaging using integrated optical sensor layers and a color camera. *Lab Chip* 2013;**13**:1593–601
69. Rennert K, Steinborn S, Groger M, Ungerbock B, Jank AM, Ehgartner J, Nietzsche S, Dinger J, Kiehntopf M, Funke H, Peters FT, Lupp A, Gartner C, Mayr T, Bauer M, Huber O, Mosig AS. A microfluidically perfused three dimensional human liver model. *Biomaterials* 2015;**71**:119–31
70. Acosta MA, Ymele-Leki P, Kostov YV, Leach JB. Fluorescent microparticles for sensing cell microenvironment oxygen levels within 3D scaffolds. *Biomaterials* 2009;**30**:3068–74
71. Kim HD, Yi SJ, Kim KC. Simultaneous measurement of dissolved oxygen concentration and velocity field in microfluidics using oxygen-sensitive particles. *Microfluid Nanofluid* 2013;**15**:139–49
72. Wang L, Acosta MA, Leach JB, Carrier RL. Spatially monitoring oxygen level in 3D microfabricated cell culture systems using optical oxygen sensing beads. *Lab Chip* 2013;**13**:1586–92
73. Dobrucki JW. Interaction of oxygen-sensitive luminescent probes Ru(phen)(3)(2+) and Ru(bipy)(3)(2+) with animal and plant cells in vitro. Mechanism of phototoxicity and conditions for non-invasive oxygen measurements. *J Photochem Photobiol B* 2001;**65**:136–44
74. Zhong W, Urayama P, Mycek MA. Imaging fluorescence lifetime modulation of a ruthenium-based dye in living cells: The potential for oxygen sensing. *J Phys D Appl Phys* 2003;**36**:1689–95
75. Polinkovsky M, Gutierrez E, Levchenko A, Groisman A. Fine temporal control of the medium gas content and acidity and on-chip generation of series of oxygen concentrations for cell cultures. *Lab Chip* 2009;**9**:1073–84
76. Adler M, Polinkovsky M, Gutierrez E, Groisman A. Generation of oxygen gradients with arbitrary shapes in a microfluidic device. *Lab Chip* 2010;**10**:388–91
77. Erickstad M, Hale LA, Chalasani SH, Groisman A. A microfluidic system for studying the behavior of zebrafish larvae under acute hypoxia. *Lab Chip* 2015;**15**:857–66
78. Mishra A, Starly B. Real time in vitro measurement of oxygen uptake rates for HEPG2 liver cells encapsulated in alginate matrices. *Microfluid Nanofluid* 2009;**6**:373–81
79. Provin C, Takano K, Yoshida T, Sakai Y, Fujii T, Shirakashi R. Low O2 metabolism of HepG2 cells cultured at high density in a 3D microstructured scaffold. *Biomed Microdevices* 2009;**11**:485–94
80. Shulman M, Nahmias Y. Long-term culture and coculture of primary rat and human hepatocytes. In: Randell SH, Fulcher ML (eds). *Epithelial cell culture protocols*. New York: Humana Press, 2013, pp. 287–302
81. Jungermann K, Kietzmann T. Oxygen: Modulator of metabolic zonation and disease of the liver. *Hepatology* 2000;**31**:255–60

82. Roy P, Washizu J, Tilles AW, Yarmush ML, Toner M. Effect of flow on the detoxification function of rat hepatocytes in a bioartificial liver reactor. *Cell Transplant* 2001;**10**:609–14
83. Tilles AW, Baskaran H, Roy P, Yarmush ML, Toner M. Effects of oxygenation and flow on the viability and function of rat hepatocytes cocultured in a microchannel flat-plate bioreactor. *Biotechnol Bioeng* 2001;**73**:379–89
84. Yuki T, Masayuki Y, Teruo O, Takehiko K, Kiichi S. Evaluation of effects of shear stress on hepatocytes by a microchip-based system. *Measure Sci Technol* 2006;**17**:31–67
85. Rashidi H, Alhaque S, Szkolnicka D, Flint O, Hay DC. Fluid shear stress modulation of hepatocyte-like cell function. *Arch Toxicol* 2016;**90**:1757–61
86. Brennan MD, Rexius-Hall ML, Elgass LJ, Eddington DT. Oxygen control with microfluidics. *Lab Chip* 2014;**14**:4305–18
87. Yoon E, Babar A, Choudhary M, Kutner M, Pyrsopoulos N. Acetaminophen-induced hepatotoxicity: A comprehensive update. *J Clin Transl Hepatol* 2016;**4**:131–42
88. Anundi I, Lahteenmaki T, Rundgren M, Moldeus P, Lindros KO. Zonation of acetaminophen metabolism and cytochrome P450 2E1-mediated toxicity studied in isolated periportal and perivenous hepatocytes. *Biochem Pharmacol* 1993;**45**:1251–9
89. Manyike PT, Kharasch ED, Kalhorn TF, Slattery JT. Contribution of CYP2E1 and CYP3A to acetaminophen reactive metabolite formation. *Clin Pharmacol Therapeut* 2000;**67**:275–82
90. Pereira CV, Nadanaciva S, Oliveira PJ, Will Y. The contribution of oxidative stress to drug-induced organ toxicity and its detection in vitro and in vivo. *Expert Opin Drug Metab Toxicol* 2012;**8**:219–37